PERGAMON

International Journal of Solids and Structures 39 (2002) 1443–1462

INTERNATIONAL JOURNAL OF SOLIDS and STRUCTURES

www.elsevier.com/locate/ijsolstr

Cracking in thin multi-layers with finite-width and periodic architectures

Joseph M. Ambrico [a], Edward E. Jones [a], Matthew R. Begley [b,*]

[a] *Department of Mechanical Engineering, University of Connecticut, 191 Auditorium Road, U-139, Storrs, CT 06269-3139, USA*
[b] *Department of Civil Engineering, University of Virginia, B228 Thornton Hall, 351 McCormick Road, Charlottesville, VA 22904-4742, USA*

Received 26 April 2001

Abstract

Many applications involve thin multi-layers comprised of repeating patterns of different material sections, notably interconnect–dielectric structures in microelectronics. This paper considers a variety of failure scenarios in systems with periodically arranged features within a single layer. Crack driving forces are presented for (i) debonding between alternating material sections in a thin film (i.e. channel and tunnel cracking at material junctions), and (ii) channel cracking in a thin uniform coating above a layer comprised of alternating sections of different materials. The effects of elastic mismatch, feature spacing, crack spacing and residual stress are illustrated for a wide range of parameters. The results presented here illustrate that residual stresses in intact sections can strongly promote cracking in adjacent layers, which is in contrast to analyses of blanket film multi-layers which predict that residual stress in adjacent layers has no effect. An important finding is that *decreasing* the relative size of low-modulus sections significantly *increases* the crack driving force in adjacent layers. The implications of these results are discussed in the contexts of critical feature spacing and the impact of incorporating low elastic-modulus sections (such as polymer dielectrics) on thermo-mechanical reliability.

Keywords: Multi-layer; Fracture; Debonding; Thin films; Periodic

1. Introduction

Previous investigations into failure of thin multi-layers are based largely on analyses of "blanket" films that are continuous and semi-infinite in length (see Hutchinson and Suo (1992) for a comprehensive review). Such idealized geometries are inappropriate for many current applications, notably microelectronics, which involve multi-layers comprised of dissimilar materials that are arranged in alternating fashion within a single layer. Adjacent layers may be either blanket films or have different alternating patterns of yet even more materials. While blanket film studies have established a useful framework for predicting failure, analyses (and experiments) without finite-sized features are not often capable of yielding insight and/or

* Corresponding author. Fax: +1-804-982-2951.
E-mail address: begley@virginia.edu (M.R. Begley).

0020-7683/02/$ - see front matter
PII: S0020-7683(01)00235-9

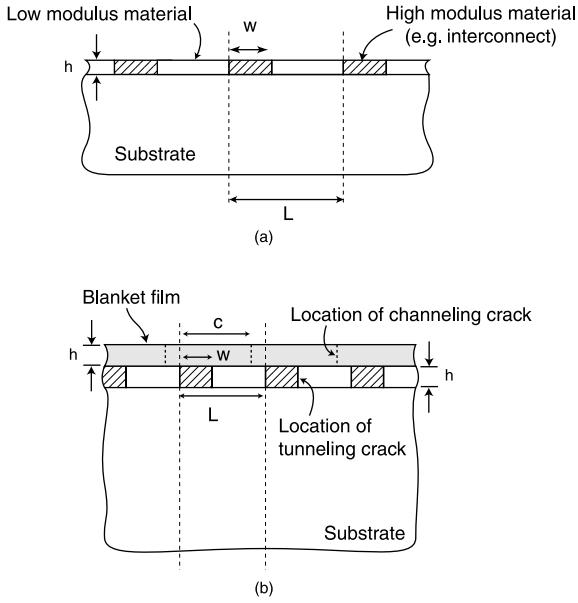

Fig. 1. Periodic thin film structures under construction: (a) single film with alternating sections of materials with different elastic properties; and (b) a blanket film (passivation layer) on top of thin alternating sections with different elastic properties.

guidance for designers charged with specifying acceptable architectures. For example, the impact of interconnect spacing on thermo-mechanical reliability is a critical concern in designing microchips, particularly as new low-modulus dielectrics are incorporated (Maier, 2001; Martin et al., 2000; Peters, 1999). An important consideration is that the interface toughness at dissimilar material junctions is usually different from (and much less than) the toughness of each material. Even when debonding is not detrimental to electrical performance, it can lead to structural ratcheting, wherein material displacements in elastic–plastic sections increase with each thermal cycle (Begley and Evans, 2001). [1] As such, there is a critical need to identify crack driving forces as a function of feature spacing, material properties, and stresses arising from deposition and thermal expansion mismatch.

Considering the growing variety of architectures and materials used in current applications, a comprehensive set of solutions for all relevant geometric arrangements and material combinations is not practical. However, significant insight can be gained by considering several prevalent architectures that are idealized as periodically arranged features of finite size, as shown in Fig. 1. These examples reveal important trends in the critical spacing between material junctions that eliminates cracking. A range of material properties is considered, with an emphasis on identifying the implications of introducing sections with low elastic moduli, as occurs when porous SiO_2 and polymers are used as dielectrics (Peters, 1999; Maier, 2000). As will be demonstrated, an important implication of including finite-sized features is that crack driving forces are strongly influenced by residual stresses in adjacent layers. This is in contrast to elastic blanket film scenarios wherein the residual stress in layers adjacent to the cracked layer has no effect (Beuth, 1992; Hutchinson and Suo, 1992). The cases considered here will be of immediate use in identifying undesirable architectural features, such as interconnect spacing and width relative to the period of the pattern.

[1] This reference considers the effect of thermal cycling on channeling crack opening; the initial flaw considered in that paper may arise from the mechanisms considered here.

The intent of this paper is to identify important trends and "rules of thumb" useful in designing fail-safe repeating architectures, and to illustrate an efficient computational approach for identifying failure scenarios in general two-dimensional architectures. Both of these purposes are demonstrated by presenting results for a wide range of feature dimensions and material properties. In many respects, the approach taken here follows the philosophy outlined by Liu et al. (2000) for developing design rules to avoid failure in integrated circuit structures. In the spirit of their paper, worst case scenarios are considered wherein it is assumed that flaws exist that are large enough to induce steady-state cracking, for which the driving force is highest. This paper utilizes a general computational framework that is capable of evaluating an enormous range of failure scenarios (Begley et al., 2001); this allows the creation failure maps that detail acceptable ranges of feature spacing and properties.

2. The mechanics of channel and tunnel cracking

In this section, we present the relevant mechanics for predicting the energy release rates for channeling and tunneling cracks at bi-material interfaces, such as those illustrated in Fig. 1. It is assumed that the out-of-plane crack length is significantly longer than the layer thickness, such that the crack driving force has reached steady state and is independent of crack length. The energy release rate for a crack tunneling or channeling at a bi-material interface is found by evaluating the following expression:

$$G_{ss} = \frac{1}{2h}\int_0^h \left[\sigma(z)(u_n^+(z) - u_n^-(z)) + \tau(z)(u_t^+(z) - u_t^-(z))\right] dz \tag{1}$$

where z is the distance along the crack (through the thickness of the film), σ and τ are the normal and shear stresses acting at the interface *before* cracking, and u_n and u_t are the normal (mode I) and tangential (mode II) crack face displacements *after* cracking. h is the film thickness in the layer containing the crack and corresponds to the crack length. The superscript $(+/-)$ denotes each side of the crack since crack face displacements will not necessarily be symmetric. In most of the scenarios considered here, the mode II contribution (i.e. the second term) turns out to be negligible compared to the mode I contribution. For blanket films with stresses generated purely through thermal expansion mismatch with the substrate, it is exactly zero.

The closed form result for a blanket film on a substrate with identical elastic properties provides a useful reference to highlight the role of elastic mismatch (Beuth, 1992) and plasticity (Beuth and Klingbeil, 1996; Begley and Evans, 2001). To set the stage for normalizations used later, the energy release rate for a blanket film with uniform film stress, σ, can be written as:

$$G_{ss} = \sigma \Delta \tag{2}$$

where Δ is the integral of the total crack opening:

$$\Delta = \frac{1}{2h}\int_0^h \left[u_n^+(z) - u_n^-(z)\right] dz \tag{3}$$

For a blanket film, the stress can be written as the sum of intrinsic stresses arising from deposition and those arising from thermal expansion mismatch with the substrate:

$$\sigma = -(1+\nu)\overline{E}\,\Delta\alpha\,\Delta T + \sigma^0 \tag{4}$$

where the plane-strain modulus of the film is $\overline{E} = E/(1-\nu^2)$; $\Delta\alpha = \alpha - \alpha_s$, where α and α_s are the coefficients of thermal expansion (CTE) of the layer and substrate respectively, and ΔT is the change in temperature from the deposition temperature (assumed to be free of thermal strain). σ^0 is the intrinsic stress

arising from sources other than CTE mismatch. Eq. (3) for a channeling crack yields (for a substrate with identical elastic properties)

$$\Delta = 1.976\frac{\sigma h}{\overline{E}} \tag{5}$$

Upon combining Eqs. (2) and (5), one obtains the well-known result (Hutchinson and Suo, 1992; Beuth, 1992):

$$G_{ss} = 1.976\frac{\sigma^2 h}{\overline{E}} \tag{6}$$

It is clear that the quantity $\sigma^2 h/\overline{E}$ is a convenient normalization for G_{ss}, as it captures the stress, thickness and modulus dependence of the energy release rate (Liu et al., 2000). In subsequent figures, energy release rates are presented in terms of $\overline{E}_1 G/\sigma^2 h$ for debonding between material sections (with $\overline{E}_1$ being the plane-strain modulus of the stiffer section), and in terms of $\overline{E}_f G/\sigma^2 h$ for channel cracking in a blanket film (with $\overline{E}_f$ being the plane-strain modulus of the film). In the limit that the physical scenario being considered reduces to a blanket film, the results asymptote to the appropriate numerical constant arising from the integration of the crack opening shape (Beuth, 1992).

While no single normalization is effective for all cases, Eq. (2) serves as the starting point to construct a useful analytical estimate of the energy release rate for a crack at a bi-material interface. It will be shown later (look ahead to Figs. 5 and 6) that this estimate is useful in accounting for the feature spacing, film thickness and elastic mismatch. An estimate of the stress acting at the interface prior to cracking (which is used in lieu of Eq. (4)) is obtained by assuming: (i) plane-strain deformation, (ii) the stress in each material section is uniform, and (iii) the total displacement of each period (consisting of two sections) is zero. The result is

$$\sigma_i = -\left\{\frac{(1+v_1)\frac{w}{L} + \frac{\Delta\alpha_2 \Delta T_2}{\Delta\alpha_1 \Delta T_1}(1+v_2)(1-\frac{w}{L})}{(1+v_1)\frac{w}{L} + \frac{(1-v_2^2)}{(1-v_1)}\left(1-\frac{w}{L}\right)\frac{E_1}{E_2}}\right\}\left[\frac{E_1 \Delta\alpha_1 \Delta T}{1-v_1}\right] \tag{7}$$

where w, E_1, and v_1 are the width, modulus and Poisson's ratio of the stiffer section; $\Delta\alpha_1 = \alpha_1 - \alpha_s$, and L is the period length. The subscript "2" refers to the corresponding properties of the compliant section; this convention is used throughout this paper. Note that the term in the square brackets is the result for the stress in a blanket film of the stiffer material. Additional details concerning the derivation of Eq. (7) are provided in Appendix A.

The crack face opening (Δ in Eq. (2)) is estimated as the average of the crack face displacements that occur in cracks in blanket films of each material. For channeling cracks, the result (used in lieu of Eq. (5)) is

$$\Delta_i = \frac{1.976}{2}\left(\frac{\sigma_1 h}{\overline{E}_1} + \frac{\sigma_2 h}{\overline{E}_2}\right) \tag{8}$$

where σ_1 and σ_2 are the stresses each material section acting to open the crack after debonding, estimated as the result for a uniform blanket film given as Eq. (4). (Equivalent expressions for tunneling cracks are constructed using the results outlined in Hutchinson and Suo (1992); it should be noted that only the constant in Eq. (8) is modified.) The estimate for the energy release rate at the bi-material interface is then constructed using Eqs. (2), (7) and (8):

$$G_0 = \sigma_i \Delta_i \tag{9}$$

The motivation for Eq. (9) should be emphasized. It is constructed by combining an expression for the stress at the interface prior to cracking, σ_i, with an expression for the crack opening after cracking, Δ_i, which is based on the average of blanket film predictions. In the limit that the material properties on both

sides of the interface are the same, it reduces to the correct expression for a blanket film on a substrate with identical properties. Using Eq. (9) to normalize energy release rates will produce results that are of the same order of magnitude, even for large mismatch ratios and large differences in the widths of each section. As is illustrated in Section 4.1, it is a highly accurate prediction for periods $L < 10h$, where h is the film thickness. For thin films (or large crack spacing), it may be off by 30–50% from the numerical results, and trends are more clearly illustrated using the normalization $\overline{E}_1 G/\sigma_1^2 h$. This is discussed in more detail in Section 4.1.

3. FEA models: energy release rate calculations

The interface stress prior to cracking and the displacements after cracking are obtained with the use of finite element models. The features considered here are illustrated in Fig. 1. The boundary conditions for the models are illustrated in Fig. 2a; the geometry is assumed to be periodic and only one period of the structure is modeled. In all cases presented here, the substrate is taken to be semi-infinite, although the FEA approach is obviously amenable to finite thickness substrates. Periodicity is enforced by requiring that the displacements on the left and right boundaries are identical. The stress in the layers is created by specifying different temperature changes and/or CTE for each layer. Intrinsic stresses may be accounted for by modifying either the CTE or temperature change such that the final stress in each layer is equal to the total stress arising from both elastic mismatch and intrinsic stress. Note that each period contains one crack; this means that cracking between alternating sections occurs only at the right-hand side of the high modulus material, since the left side coincides with the period boundary. Energy release rates for debonding along both sides of a feature are necessarily lower. In some scenarios self-similarity can be exploited to convert the single crack (per period) result to the result for both interfaces debonding (Delannay and Warren, 1991).

Stress singularities are present at crack tips and at locations where material intersections intersect a free surface or a different material. The strength of each singularity depends on the properties of all the materials surrounding the crack. This has been well documented for cracks along bi-material interfaces (Hutchinson and Suo, 1992) and for singularities arising from the intersection of material interfaces with free surfaces (Ghahremani and Shih, 1992). While various schemes can be constructed to explicitly capture the singularity via special elements, a "brute force" approach is taken here wherein a focused radial mesh of conventional eight-node quadrilateral elements is included at every material intersection *within* the period. This approach can be easily justified on the grounds that: (i) different singular elements would be required for each material combination (since the strength of singularity depends on elastic mismatch), and most importantly, (ii) accurate, convergent results can be obtained with reasonable computational expense without recourse to specialty elements.

An example of the resulting mesh pattern (with a very low mesh density and a reduced substrate thickness for illustration purposes) is illustrated in Fig. 2b. Note that radial focused meshes are present at all interior material corners and the crack tip (if relevant). Convergence studies demonstrated that focused meshes at the material junctions on either edge of the period were unnecessary to obtain convergent results. The present results are limited to the case of a semi-infinite substrate, in that the thickness of the substrate is 25–50 times larger than the thickness of either layer (note Fig. 2b is not to scale). Convergence tests performed both here and elsewhere (Beuth, 1992) have illustrated that this is sufficient to generate results that are independent of substrate thickness.

Since the exact singularity is not captured with a single special purpose element for arbitrary combinations of material properties, there is little to no motivation for using a mesh with collapsed (or triangular elements) at bi- or tri-material corners. Put another way, the details of the model's corner geometry are unimportant provided they are localized within a distance that is small compared with the feature dimensions. To facilitate efficient mesh generation, the corner geometry is modeled as a circular "hole" with a radius that is several orders of magnitude smaller than the smallest relevant film dimension (thickness or

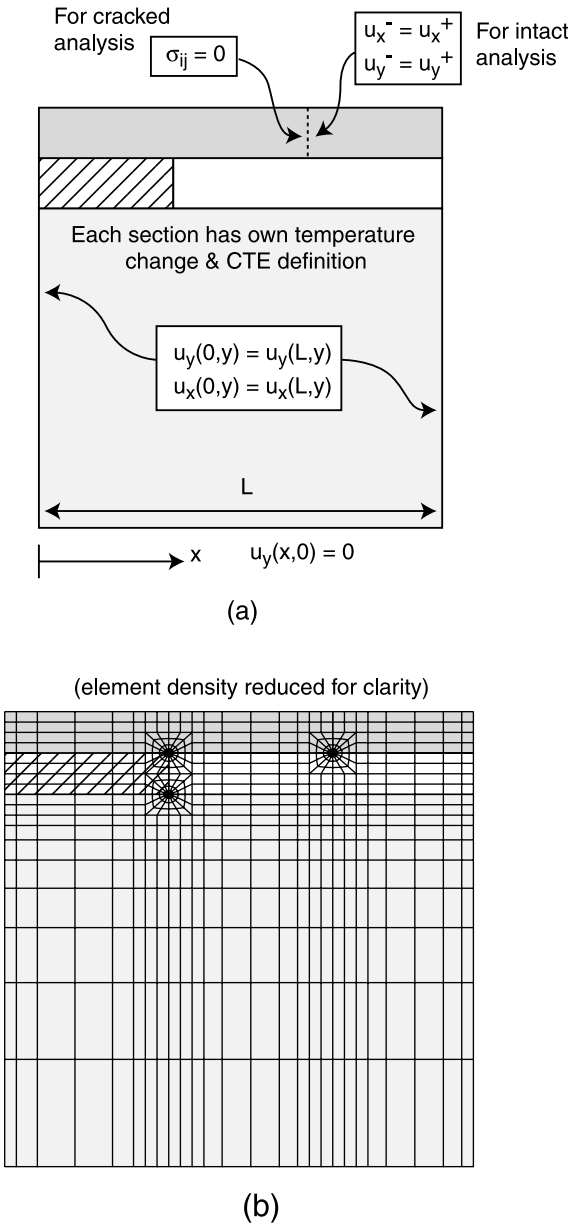

Fig. 2. Schematic diagram of the FEA boundary conditions and mesh with focused radial meshes at interface corners and the crack tip, for the scenario illustrated in Fig. 1b (figures are not to scale).

width). Each material block has a small quarter circle cut from each corner; the corner of each feature has the same notch radius, such that a fully circular hole is created. It must be emphasized that the artificial hole has *absolutely no effect* on the resulting energy release rate computations, since the hole radius is several (in this case, three) orders of magnitude smaller than relevant geometric dimension. The details of the corner geometry are unimportant on physical grounds because for appropriate film thickness (on the order of

microns) the absolute size of the first few elements within the focused region is kept in the nanometer range. Hence, the non-convergent region near the singularity (i.e. the first few elements near the corner) has a negligible effect on the energy release rate calculation. This has been verified by an extremely wide variety of convergence studies on appropriate mesh parameters, including the hole radius and the size, number and distribution of the elements near the singularity (Begley et al., 2001).

This meshing technique has the significant practical advantage of using a single mesh-generation strategy for arbitrary combinations of material sections. Moreover, the models consist only of material *interfaces* which can be debonded. Corner points do not exist in the FEA model and do not need to be dealt with explicitly. This alleviates headaches associated with developing complicated nodal constraints where four materials meet at a single corner (Begley et al., 2001). The results in this paper were generated using more than 200 individual meshes (one for each individual combination of film thickness, period, and material section widths). Using automated mesh-generation schemes, model creation is fairly rapid (on the order of a minute) and computation times were generally on the order of 2–3 min (on a 500 MHz/512 MB RAM DEC Alpha workstation). Additional details regarding the number of elements and strategies for model creation and solution are detailed in Begley et al. (2001).

4. Results for crack driving forces

4.1. Debonding at periodic material junctions within a single thin layer

Crack driving forces for interface debonding between two different material sections within a single layer are shown in Fig. 3. The figure illustrates the role of the relative width of the sections for several elastic moduli ratios. For each case, the thermal strain in each section is identical and the film thickness-to-period ratio, h/L, is 0.01. In all of the cases considered in this section, the modulus of the stiffer section, E_1 is taken to be identical to the substrate modulus, E_s, with $v_1 = v_2 = 0.3$, and $v_s = 0.2$. As the width of one section becomes significantly larger than the other, the results asymptote to the result for a blanket film. Since the stiffer section modulus is used in the normalization, the results asymptote to 1.976 for $w/L \to 1$. For $w/L \to 0$, the results asymptote to approximately $1.976\overline{E}_2/\overline{E}_1$; this is not an exact result because the

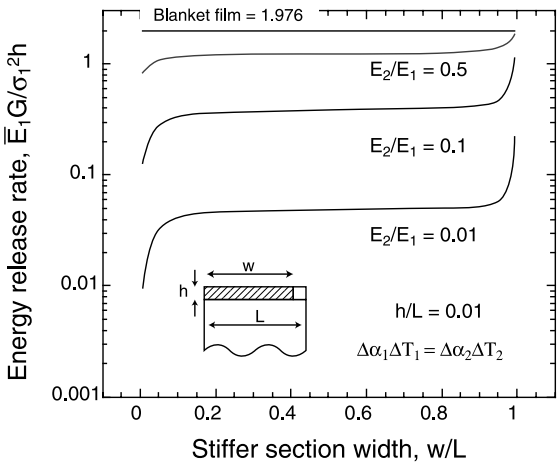

Fig. 3. Energy release rates for channeling cracks between alternating sections as a function of section widths (w/L is the length of the stiffer section) for several elastic moduli ratios, equal thermal strains and $h/L = 0.01$.

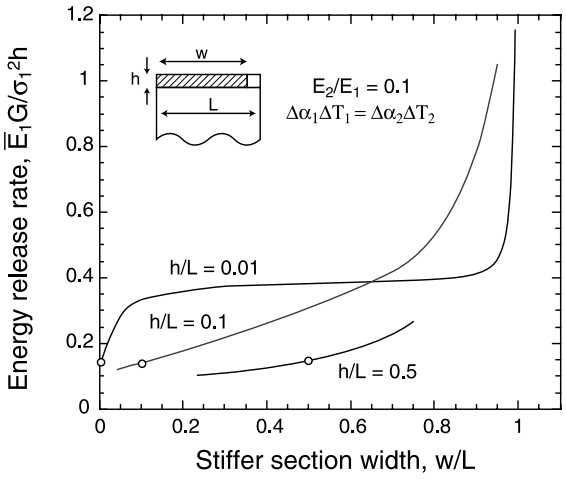

Fig. 4. Energy release rates for channeling cracks between alternating sections as a function of section widths (and period lengths) for several film thicknesses (h/L) and equal thermal strains.

substrate has different elastic properties than the blanket compliant film. It is anticipated that results for cases where the substrate has significantly different elastic properties can be fairly well approximated by adjusting the present results using those tabulated in Beuth (1992).

It can be seen in Fig. 3 that the crack driving force is relatively insensitive to the section lengths, except near the extremes where one section is much larger than the other. For thin films (compared to the period), the shear transfer length is small compared to the section widths and the material junctions behave as isolated interfaces. The energy release rate is much more sensitive to section width when the width of either section approaches the film thickness. This is illustrated in Fig. 4, which depicts the results for equal thermal strains and one ratio of elastic moduli, $E_2/E_1 = 0.1$. For thicker films (compared to the period), the width of either section is comparable to the film thickness and the two interfaces on either side of the smaller section interact. Put another way, the shear transfer length (which scales with the film thickness) is comparable to the width of each section and the transition between the two extremes is much more gradual. Thin film scenarios where the interfaces are very close together, i.e. when the section widths are comparable to the film thickness, will be discussed in more detail in Section 5.

It should be kept in mind that the normalization implies that the driving force scales with film thickness. The decrease in ERR as h/L is varied for a constant value of w/L can be interpreted as the effect of an increasing crack density per unit thickness. Note again that each period contains one crack, hence L is equivalent to the crack spacing. Unfortunately, the problem affords a number of choices for normalization, such as w/L, h/L or w/h, and there does not appear to be a convenient choice that elucidates all trends. For example, the open circles in Fig. 4 are all for cases where the width of the stiffer section equals the film thickness, i.e. $w/h = 1$. For all of these points, the width of the compliant section is large enough (i.e. the crack density is small enough) to effectively prevent interaction between stiff sections, and the energy release rate remains relatively constant for the different cases.

The effect of crack density, reflected through the ratio of film thickness-to-period length h/L, is illustrated in Fig. 5 for a variety of elastic mismatch ratios and section widths. The top curve in Fig. 5a is the result for a uniform film with multiple cracks, as solved by Delannay and Warren (1991), Thouless (1990) and Schulze and Erdogan (1998) and reviewed by Hutchinson and Suo (1992). It is clearly seen in Fig. 5a that for all film thickness (and hence crack densities), decreasing the elastic modulus of one of the sections

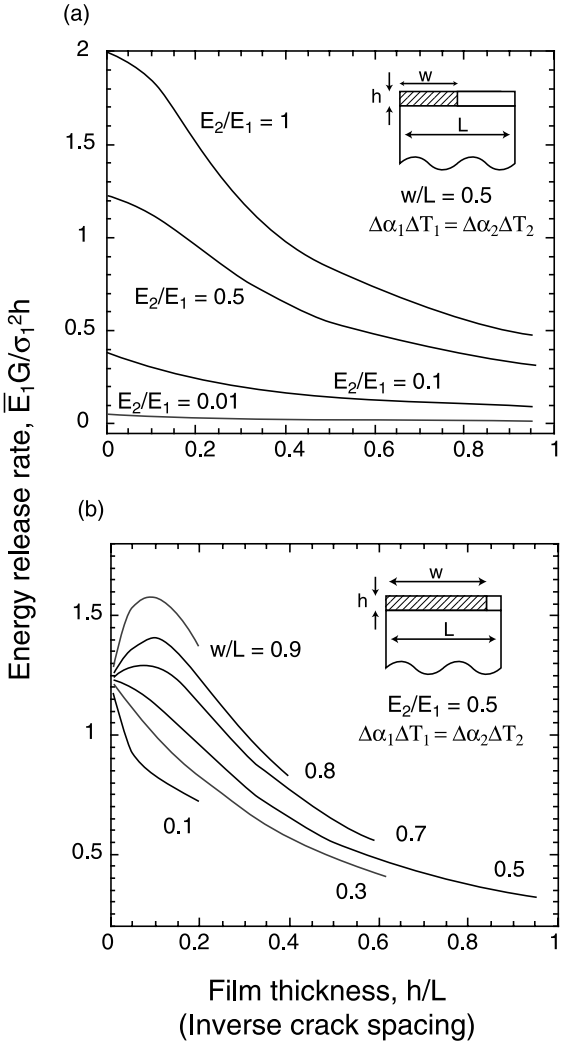

Fig. 5. (a) Energy release rates for channeling cracks as a function of crack spacing (the period length L is the distance between cracks) for several elastic mismatch, equal thermal strains and $w/L = 0.5$. (b) Energy release rates for channeling cracks as a function of crack spacing for several section widths, equal thermal strains and elastic mismatch ratio $E_2/E_1 \sim 0.5$.

decreases the energy release rate. This is a result of the fact that the stress in one of sections decreases with modulus (note that equal thermal strains are shown). Fig. 5b illustrates that for film thickness (or crack spacing) where $h/L > 0.1$, increasing the crack density decreases the energy release rate. Note the initial rise in the curves for small values of h/L and $w/L > 0.5$. This is because the compliant section width *relative to the film thickness* is decreasing. For low crack densities, this initially drives the result closer to the case of a blanket film of the stiff material. Eventually, the drop in energy release rate with increasing crack density (h/L) effect takes over.

For significant crack densities (for crack spacing less than 10 times the film thickness, i.e. $h/L > 0.1$), the results can be effectively collapsed into a "master" curve by using the normalization outlined in Section 2.

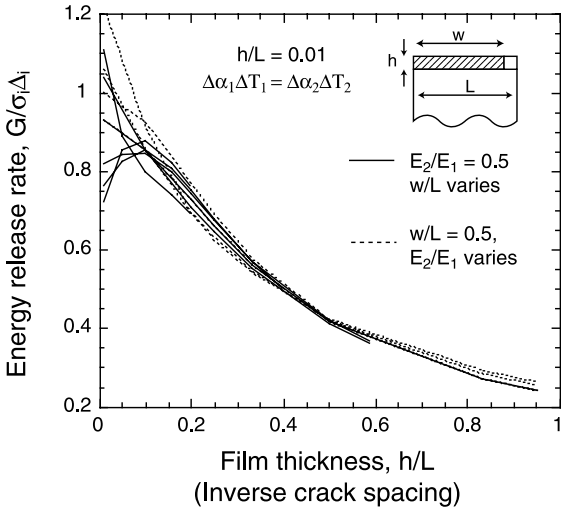

Fig. 6. Energy release rate for channeling cracks versus crack density for all cases of elastic mismatch and section widths using the $G_0 = \sigma_i \Delta_i$ (defined by Eq. (6)); the normalization incorporates w/L and E_2/E_1 and collapses the data from Fig. 5 into a single curve.

This is illustrated in Fig. 6. Note that the spread for the wide range of cases is less than 10% for $h/L > 0.1$, implying that both the dependence on w/L and the dependence on E_2/E_1 is effectively captured by the normalization. This is a useful single result that can be used to predict the effect of crack density for a wide range of film thickness, feature spacing and elastic mismatch. The spread in the data for small h/L is primarily a result of the fact that Eq. (7) inaccurately predicts the interface stress. For $h/L \to 0$, deviations from unity reflects the fact that the substrate has different elastic properties from the compliant layer. Fig. 6 demonstrates that Eqs. (2), (7) and (8) provide an excellent prediction for thicker films and higher crack densities.

It should be noted that the ratio of the thermal strains in each section has a significant effect as well. This is illustrated in Fig. 7, which shows results for equal section widths and several values of elastic mismatch. The open circles in Fig. 7 are cases with thermal strain and elastic mismatch ratios that are plotted in Fig. 3 as a function of w/L. Decreasing the thermal strain in the compliant section drives the result towards the asymptotic limit of a stress free compliant section. For sufficiently large thermal strain ratios, the stress in the compliant section dominates and the results scale with $\sigma_2^2 \sim (\Delta\alpha_2 \Delta T_2)^2$ rather than σ_1^2. This explains the transition to a straight line on the log–log scale with slope $= 2$. It should be noted that decreasing the modulus (accomplished via changing the material) is usually accompanied by a change in CTE, such that the effects shown in Figs. 3 and 7 may offset one another to varying degrees.

4.2. Tunnel cracking at periodic material junctions in an embedded layer

Results are presented in Fig. 8 for a crack tunneling between two dissimilar materials in a single layer with a passivation layer on top, as illustrated in Fig. 1b. We limit our attention to a film thickness, thermal strain ratio and passivation layer properties appropriate to interconnect–dielectric structures, and focus on the role of stiff section (interconnect) width (w/L) and modulus of the compliant section (dielectric). The results in Fig. 8 exhibit similar trends to those shown in Fig. 3 for the channel cracking scenario. Here, the elastic mismatch with the substrate is $E_s/E_1 = 1.3$. Generally speaking, the role of various parameters is

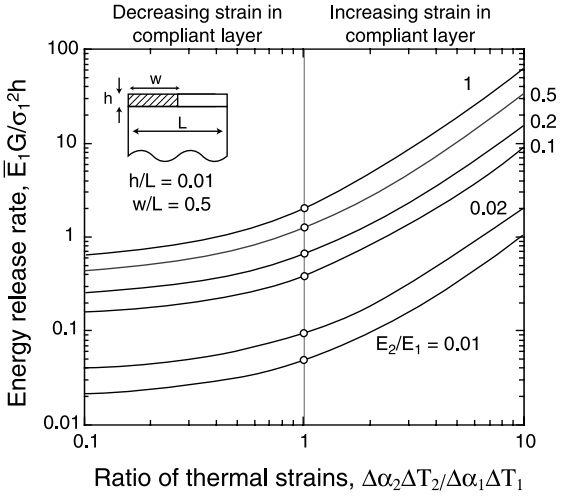

Fig. 7. Energy release rates for channeling as a function of thermal strain ratio $\Delta\alpha_2\,\Delta T_2/\Delta\alpha_1\,\Delta T_1$ for several values of elastic mismatch, $w/L = 0.5$ and $h/L = 0.01$.

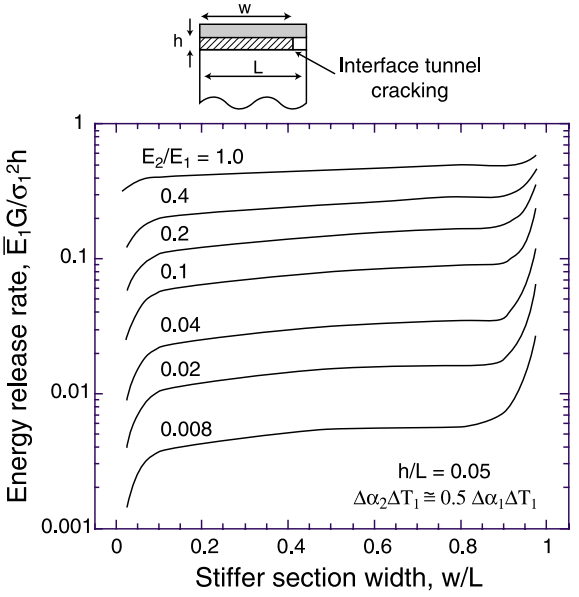

Fig. 8. Energy release rates for tunneling cracks as a function of material junction spacing for several values of elastic mismatch, $h/L = 0.05$ and a thermal strain ratio of $\Delta\alpha_2\,\Delta T_2/\Delta\alpha_1\,\Delta T_1 \sim 0.5$. The ratio of the top layer modulus and substrate modulus to that of stiffer section (of width w/L) is $E_s/E_1 = 1.3$.

the same, with crack driving forces being relatively insensitive junction spacing over a wide range for thin films. Increasing the modulus mismatch (by decreasing the modulus of the dielectric) leads to lower crack driving forces (*for constant thermal strain in the compliant section*).

4.3. Channel cracking in a blanket layer deposited above periodically spaced features

It is of particular interest to determine the effect of feature geometry on cracking in adjacent layers, and it is in this scenario that we see the most interesting results. The geometry under consideration is illustrated in Fig. 1b, i.e. a channel crack in the top blanket layer. Again, we restrict our attention to groups of material properties relevant to interconnect–dielectric structures and focus on the role of feature spacing and residual stress. Fig. 9 illustrates the crack driving force as a function of crack location for several feature widths. Relevant material properties are contained in a table in the figure. The results are normalized by the result for a blanket film on a substrate with identical elastic properties. Naturally, the crack driving force is higher when the crack is located over the section with lower modulus, as the crack tip intersects a more compliant material. Note that $c/L = 0$, 1 and w/L correspond to a crack directly over the material interface in the underlying layer and hence yield the same value.

For cracks over stiff sections of finite width, the crack driving force can be near or equal to zero. Very small or zero energy release rates are a result of warping of the stiffer sections, where the more heavily stressed stiff sections curl near the edges. This warping leads to total or partial crack closure in the adjacent layers, which eliminates or significantly reduces the crack driving force. The effect is most pronounced for stiff sections with smaller aspect ratios ($w/h = 2$, 6, corresponding to $w/L = 0.1$, 0.3) since the curling at the edge of the section is close to the adjacent crack. The effect is less pronounced for wide stiff sections, as the curling deformation is too far away to influence the crack. For $w/L = 0.9$ (corresponding to $w/h = 18$), one obtains the appropriate blanket film results. Even for these cases, the energy release rate may be an order of magnitude smaller than that for a crack over a blanket film of compliant material, due to compliance differences (Hutchinson and Suo, 1992; Beuth, 1992).

The warping of the stiffer section (and resulting crack closure) varies systematically with stiffer section length and crack location. This is somewhat obfuscated in the scaling of Fig. 9; no clear trend is imme-

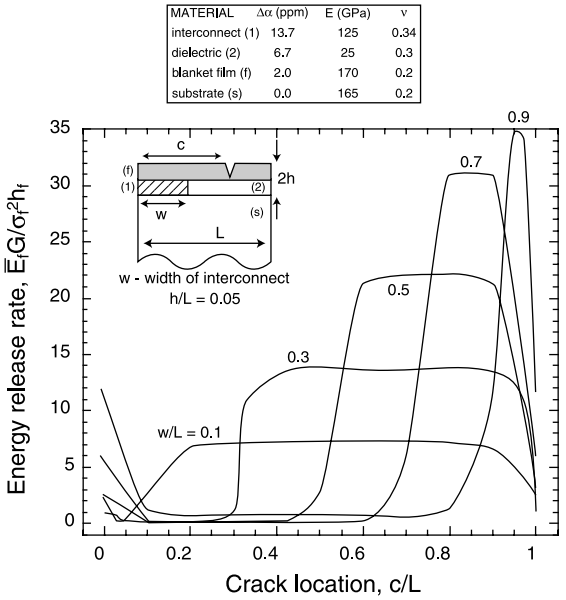

Fig. 9. Energy release rate for a channeling crack above alternating material sections, as a function of crack location and feature spacing for material properties representative of an interconnect/dielectric structure.

diately discernible at the end points ($c/L = 0$ and 1). However, calculations for these locations (corresponding to a crack over the material junction) illustrate that the ERR is a smooth non-monotonic function of w/L. For the chosen system, the ERR is a minimum at $w/L \sim 0.3$–0.4; warping of shorter sections does not create displacements large enough to close the crack, while longer sections prohibit warping. It should be noted that this discussion is strictly applicable only for the dimensions and material properties shown in Fig. 9; changing layer thickness, modulus or CTE values may eliminate crack closure effects. Unless very large changes are considered, however, the curling deformation is sufficient to drastically reduce the ERR in these scenarios.

The more striking result is that the maximum crack driving force (i.e. for a crack over the compliant section) is *significantly higher* than the result for a channeling crack over a blanket film made of the compliant material. Moreover, the crack driving force increases as the width of the compliant section decreases. This is illustrated in a dramatic fashion in Fig. 10, which depicts the crack driving force for a crack at the midpoint of the compliant section. This crack location is a convenient reference point, as it differs by only a few percent from the maximum energy release rate for any crack location (see Fig. 9). The independent variable is chosen as the thickness of the compliant section, $t/h = 1 - w/L$, in order to illustrate trends for narrow compliant sections. Clearly, the increase with decreasing compliant feature width is a result of the residual stresses present in the layers beneath the crack. Note in Fig. 10 that, in the absence of residual stress, the driving force transitions between the two expected limits—i.e. the results for a blanket film on a substrate of either modulus. These results have significant implications for device reliability, as it implies that increasing the density of interconnects increases the likelihood of cracking in adjacent layers. Critical feature spacing and residual stress levels can be identified directly from Fig. 10; this is discussed in detail in Section 6.

At first glance, it is surprising that the crack driving force continues to increase to such extremely narrow feature sizes and that it is significantly higher than the result for blanket films. One would expect that the driving force to fall as the width of the compliant section becomes small and that the results would reduce to the result for a film on a blanket film of the stiffer material. The results do follow this asymptote, yet do so at remarkably small compliant section widths. The details of small section sizes and physical explanations for the abrupt transition (note that a log scale is used) on the left of Fig. 10 are the focus of the next section.

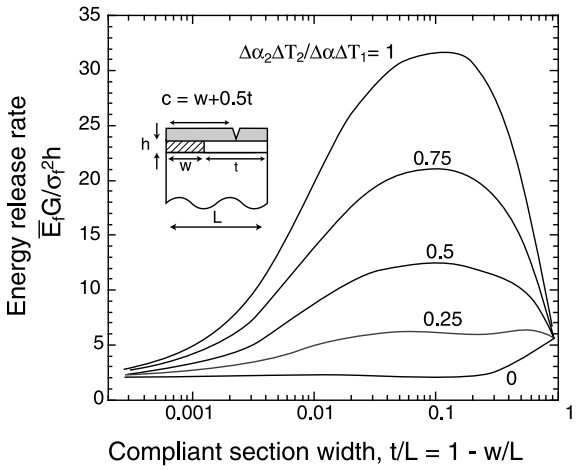

Fig. 10. Energy release rates for a crack located above the midpoint of the compliant section as a function of compliant section width, for a representative set of elastic moduli and several values of residual strain in the stiffer section.

5. Asymptotic analysis for small feature widths and the role of residual stress in adjacent layers

The behavior of the previous numerical solutions can be understood and verified by an alternative approach that captures the asymptotic behavior of very narrow sections. Consider the cases illustrated in Fig. 11: very small widths of one material sandwiched between larger sections of a different material. In the limit that the thin section width is small compared to the film thickness, the stress distribution through the width of the small section is nearly uniform and shear stresses are absent. In this case, the effect of the small region can be predicted via a crack bridging model. The system behaves as a crack in a uniform film bridged by linear springs whose stiffness is determined by $\delta = t\sigma_b/\overline{E}_p$, where δ is the total crack opening, σ_b is the bridging stress acting between the crack faces, t is the width of the small section and $\overline{E}_p$ is its plane-strain modulus.

For simplicity and to allow the use of standard linear elastic fracture mechanics results we assume that the films and substrate have the same elastic properties, except for the compliant section. The governing

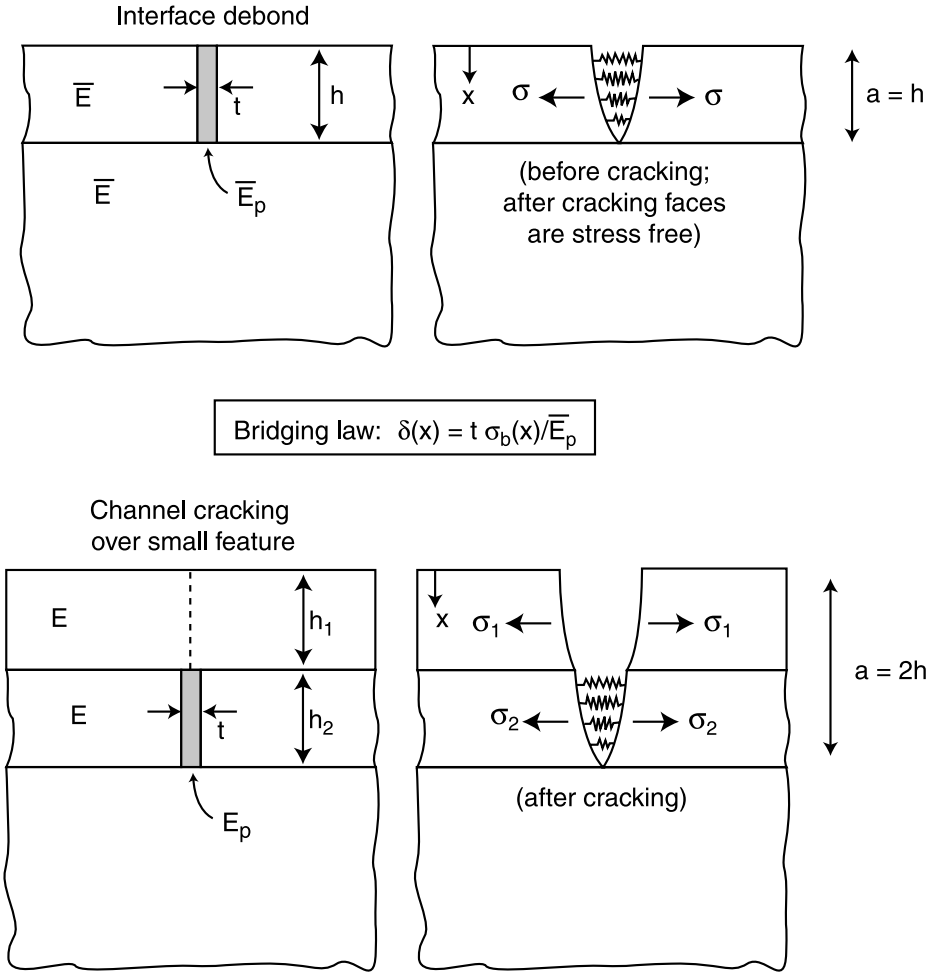

Fig. 11. Schematic illustration of the crack bridging models applied to model the results for very thin compliant sections.

equation for σ_b is derived by equating the total crack opening to the sum of the opening due to the applied load and the crack closure due to the bridging tractions. The resulting normalized integral equation is

$$\frac{t\overline{E}}{a\overline{E}_p}\Sigma(\bar{x}) + \int_{h/a}^{1} \Sigma(z)H(z,\bar{x})\,dz = f(\bar{x}) \tag{10}$$

where $\bar{x} = x/a$, $\Sigma = \sigma_b/\sigma_a$, σ_a is the applied load, and $H(z,\bar{x})$ is the Green's function specifying the crack opening at $\bar{x}$ due to a point force at z. $f(\bar{x})$ represents the crack opening profile due to a unit applied load. After solving using conventional numerical techniques (Begley and McMeeking, 1995), the resulting bridging stress and crack opening displacements can be used with Eq. (1) to directly compute the energy release rate.

For the single film scenario, the entire crack is bridged by the thin layer and the lower limit is $h/a = 0$ (Eq. (10)). Results are shown in Fig. 12 with relevant FEA results superimposed. The limit that $t\overline{E}/h\overline{E}_p$ goes to zero corresponds to a vanishingly thin section. In this case, the bridging stress distribution becomes uniform and is equal to the stress in the film, and the intact opening displacement goes to zero. This corresponds to the case of a blanket film with uniform residual stress. After cracking, the crack opening displacement is simply that of an edge crack in an isotropic body. Increasing $t\overline{E}/h\overline{E}_p$ corresponds to either increasing the thickness of the small section or to decreasing its modulus. Both have the effect of decreasing the energy release rate. In the extreme limit of a zero modulus, the energy release rate goes to zero as no stress is generated in the increasingly compliant layer between the larger sections—the film is effectively cracked before the bridging ligaments are released. The most significant aspect of these results is that both the asymptotic and numerical analyses clearly demonstrate that *extremely* small sections (compared to the film) are required to reach the asymptotic limit of a blanket film.

For a channel crack above a thin section (see Fig. 11), the same approach can be used to illustrate the effect of a vanishingly small section underneath the crack in the top film. In this scenario, the crack is defined as running through *both* the top and second layers. The lower limit in Eq. (10) in this case corresponds to the top layer thickness normalized by the thickness of both layers, i.e. $h/a = h_1/(h_1 + h_2) = 1/2$. The crack is bridged over the second layer with linear springs again dictated by the properties of the

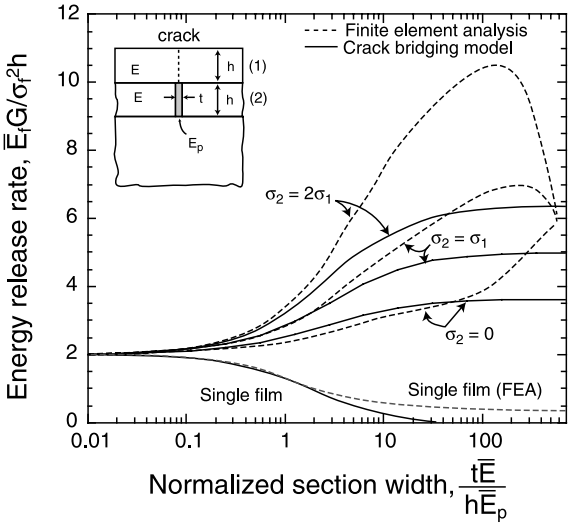

Fig. 12. Energy release rates as a function of compliant section width and modulus as predicted from an integral equation approach; results from appropriate FEA models are superimposed.

small section. Results for this scenario are shown in Fig. 12 as well. Decreasing the small section's thickness (or increasing its modulus) leads to identical results for an unbridged crack running through the top layer and arresting at the second layer. As $t\overline{E}/h\overline{E}_p$ is increased, the crack opening at the top edge of the bridging zone (i.e. the bottom of the crack in the top layer) increases and the energy release rate for a crack in the top layer increases. The upper limit corresponds to the scenario where the compliant thin sections opens as an unbridged crack and the results become independent of its thickness and/or stiffness.

The agreement between the integral equation results and FEA model is better for cases where there is a stress in the second layer. When the compliant section is small, the strain energy in adjacent sections is also released, leading to significant increases in the crack driving force when the adjacent layer is under significant stress. These considerations explain the results shown in Figs. 10 and 12, wherein the driving forces are larger than those in a blanket film of either material.

It is clear that the bridging model predicts the same abrupt increase in energy release rate with increasing compliant section width. The important conclusion is that extremely small compliant sections are required to asymptote to the blanket film result (note that a logarithmic scale is used in Fig. 12). Sophisticated discretization schemes that more accurately capture the opening near the edge of the bridging zone will most likely improve the agreement shown in Fig. 12, but are beyond the scope of this comparison.

6. Critical feature spacing and residual stresses: implications for device design and reliability

6.1. Critical junction spacing for cracking within a layer: tunnel and channel cracks

The presented results can be used to determine critical relationships between feature spacing, film thickness and stress levels to prevent interface debonding between alternating material sections. This is accomplished via equating the energy release rate to the interface toughness, Γ_i. For example, upon replacing $\overline{E}_1 G/\sigma_1^2 h$ with $\overline{E}_1 \Gamma_i/\sigma_1^2 h$ in Fig. 3, the curves represent the maximum allowable junction spacing (w/L) for a given residual stress and material toughness combination. The same holds true for Fig. 4 (channel cracking for various film thicknesses) and Fig. 8 (tunnel cracking). It is apparent the critical film spacing is a strong function of interface toughness. (This may be easier to see if one rotates these figures 90° to make the normalized interface toughness the independent variable.)

The flat portions of Figs. 3 and 8 indicate that the crack driving force is relatively insensitive to feature spacing (w/L) over a wide range. (Presumably, the sensitivity of the crack driving force to feature spacing is not a strong function of the thermal strain in each section.) Put another way, there is an essentially constant critical interface toughness for a given elastic mismatch ratio that allows a wide range of feature spacing. This is illustrated by plotting energy release rate for a given junction spacing versus elastic mismatch, as is done in Fig. 13. For any spacing beneath $w/L = 0.5$, the region above the curves corresponds to intact interfaces, while interface toughness values beneath the curves will result in interface debonding. Similar curves can be generated for other junction spacings, although it is clear from Figs. 3 and 8 that the results will be nearly identical to Fig. 13 (except for w/L close to unity or zero).

One of the primary motivations for these analyses is to determine the impact of incorporating new compliant sections into multi-layers, such as polymer dielectrics. It is clear from Fig. 13 that if a compliant section can be introduced without increasing the residual strain in the section, a smaller interface toughness is required to prevent cracking. However, changing to a lower modulus material usually involves an increase in thermal expansion coefficient. This implies that the decrease in required interface toughness is not as dramatic as that illustrated in Fig. 13, which depicts results as a function of mismatch for a *constant* thermal strain ratio. Obviously, if changing materials involves a large enough increase in thermal expansion coefficient, the benefit of introducing a more compliant material is lost and a larger interface toughness is required.

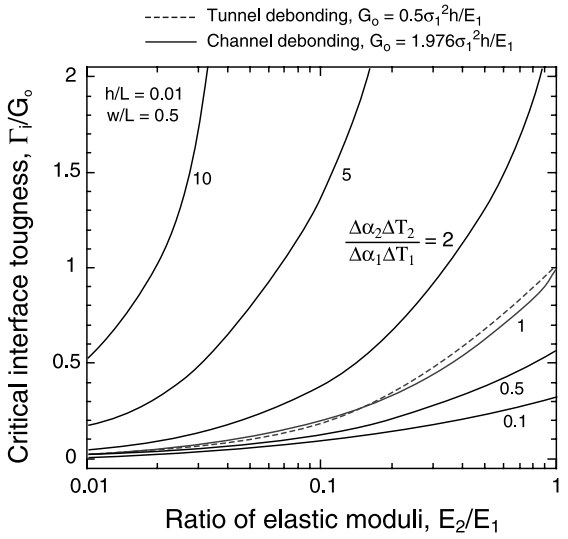

Fig. 13. Critical film toughness (required to prevent cracking) as a function of elastic mismatch for several ratios of thermal strain. Regions above the curves correspond to no debonding, while those below correspond to debonding at the interface.

6.2. Critical junction spacing to prevent cracking in adjacent layers

Figs. 10 and 12 indicate that the critical compliant section width to prevent cracking in adjacent layers is a strong function of film toughness. Again, critical relationships can be determined by replacing the energy release rate with the film toughness, i.e. replacing $\overline{E}_f G/\sigma_f^2 h$ with $\overline{E}_f \Gamma_f/\sigma_f^2 h$. Failure is avoided altogether if the film toughness is greater than the maximum energy release rate (for *any* crack location) and residual strain (and thus stress) in adjacent layers is kept beneath a critical value. Fig. 14 shows a failure map relating allowable thermal strain ratios for a given film toughness. This figure is created by cross-plotting the

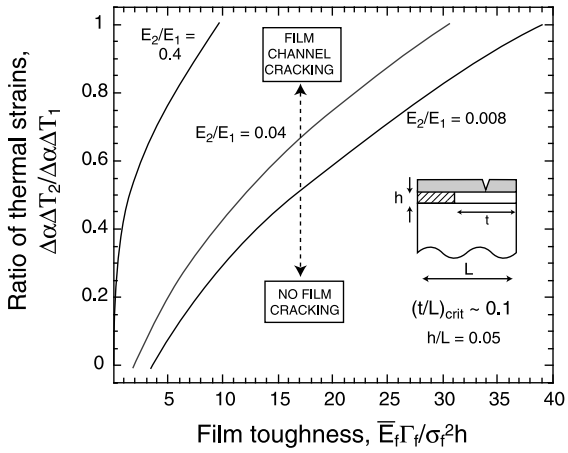

Fig. 14. Critical thermal strains to prevent cracking in passivation layer as a function of film toughness, for several elastic mismatch cases. The compliant section width is taken to be $t/L = 0.1$ and the crack location is in the middle of the compliant section (see Figs. 9 and 10).

maximum values of $\overline{E}_f G/\sigma_f^2 h$ in Fig. 10 with the thermal strain ratio for each case. Cracking will not occur if the thermal strain (or residual stress) in the adjacent layers is limited to the left of the curve. Results for a range of compliant section modulus are illustrated as well; the compliant section width is taken to be $t/L = 0.1$ since this is approximately the value where the maximum crack driving force occurs. Note that decreasing the compliant section modulus requires a larger film toughness to prevent cracking.

The range of acceptable compliant section widths for given values of residual stress and film toughness are shown in Fig. 15. These envelopes are created by determining the range of t/h where the crack driving force exceeds the film toughness from Fig. 10. For no residual stress, any compliant section widths are allowable provided that the toughness exceeds the driving force corresponding to adjacent blanket films of either material. Results for blanket films for a wide range of elastic mismatch are available (Beuth, 1992), with the assumption that the adjacent layer thickness does not strongly influence crack driving force.

6.3. Implications of elastic mismatch and thermal strains

Figs. 13–15 illustrate critical relationships than can be used to determine critical feature spacing, elastic properties and residual stresses to prevent both interface debonding and cracking in adjacent layers. It is reasonable to expect that the results will be applicable to scenarios where layers further removed from the architectures considered here are not significantly different from properties considered here. As such, it is anticipated that the relationships illustrated here can be used to develop rules of thumb for such critical values in more complex architectures.

Generally speaking, low-modulus sections decrease the likelihood of interface debonding, provided the CTE is comparable to that of the stiffer section. Changing the size of the compliant section has a relatively small effect for this type of failure. However, small sections with low moduli generally promote cracking in adjacent layers, in that they allow the release of strain energy in higher stressed sections. As such, small compliant sections should be avoided, as they may significant increase the driving forces for cracking in adjacent layers. Finally, the general analysis code used here (which is capable of analyzing a wide variety of feature sizes and including arbitrary material combinations) is of considerable use in evaluating likely failure modes.

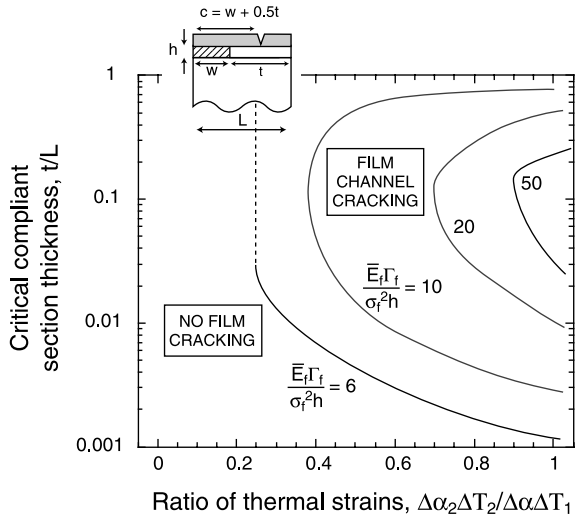

Fig. 15. Allowable complaint section widths for several values of film toughness; points to the right of the curves represent scenarios where a channeling crack will form, while those to left will prevent cracking.

7. Summary

Several failure scenarios have been studied to elucidate the effect of a very wide range of feature dimensions and material properties on cracking in multi-layers with finite-sized features. The results can be used to predict critical feature spacing or material mismatch that improves mechanical reliability by eliminating interface debonding or cracking in adjacent layers. Several key conclusions have been noted, including:

- For thin films (large crack spacing), the crack driving force for *interface debonding* is a relatively weak function of feature widths, except near the extremes where one section is much smaller than the other. Elastic mismatch between the sections and thermal strains play a much larger role than feature width (see Fig. 13).
- Residual stresses in adjacent sections increase the crack driving force for channeling cracks, in many cases significantly above the value predicted from blanket film analyses. Small compliant sections should be avoided, as they allow for the release of significant strain energy in higher stressed sections.
- An effective meshing strategy allows a wide range of failure scenarios to be evaluated with arbitrary feature dimensions and elastic mismatch. This is critical to determining important effects that are not predicted via analysis of blanket films.

Acknowledgements

The authors wish to thank Christopher J. Begley of TCA Solutions, LLC for the mesh-generation strategy and algorithms used in this paper. We also to thank Jun He of the Intel Corporation for many helpful discussions. The support of the National Science Foundation via award number CMS-9984517, is gratefully acknowledged.

Appendix A

The stresses on the interface between different material sections prior to cracking can be estimated from an elasticity model of a bi-material plate of unit width, as illustrated in Fig. 16. The total plate length is equal to the period length (L) and the thickness is equal to the film thickness (h). The following assumptions are made to develop the model: (i) the stresses in each section are uniform with no shear stresses and $\sigma_z = 0$, (ii) the film is in a state of plane strain, and (iii) there is zero net change in the period length. The plane-strain assumption requires that the total strain in each section in the y-direction is equal to zero:

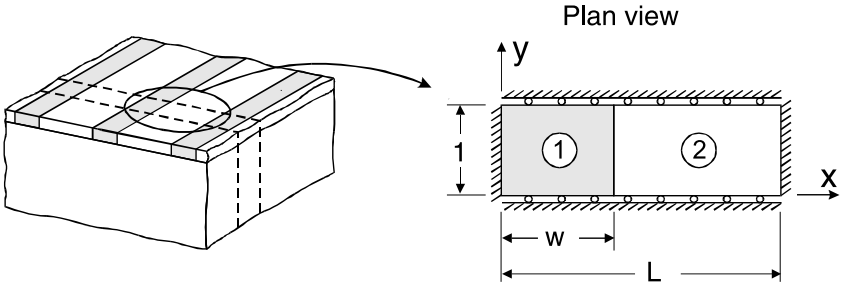

Fig. 16. Schematic illustration of the bi-material plate model used to derive Eq. (7) in the main body of the paper.

$$^{1}\varepsilon_y = {}^{2}\varepsilon_y = 0 \tag{A.1}$$

where the left superscript denotes each section. No change in the period length requires that the x-direction displacements sum to zero:

$$^{1}\varepsilon_x w + {}^{2}\varepsilon_x (L - w) = 0 \tag{A.2}$$

At the interface, equilibrium requires that the x-direction normal stresses are equal, i.e. $^{1}\sigma_x = {}^{2}\sigma_x = \sigma_x$. Standard elastic relations are then used to replace the strain terms in Eqs. (A.1) and (A.2) with the appropriate stress terms; Eq. (A.1) becomes:

$$\frac{^{1}\sigma_y}{E_1} - \nu_1 \frac{\sigma_x}{E_1} + \alpha_1 T = \frac{^{2}\sigma_y}{E_2} - \nu_2 \frac{\sigma_x}{E_2} + \alpha_2 T = 0 \tag{A.3}$$

while Eq. (A.2) yields

$$\left[\frac{\sigma_x}{E_1} - \nu_1 \frac{^{1}\sigma_y}{E_1} + \alpha_1 T\right] w + \left[\frac{\sigma_x}{E_2} - \nu_2 \frac{^{2}\sigma_y}{E_2} + \alpha_2 T\right] (L - w) = 0 \tag{A.4}$$

Eqs. (A.3) and (A.4) can be solved for the interface normal stress σ_x. The result is given as Eq. (7) in the main body of the paper.

References

Begley, C.J., Begley, M.R., Ambrico, J.M., Jones, E.E., 2001. An efficient computational approach for predicting cracking in 2-D multi-layers with finite-sized features, in preparation.

Begley, M.R., Evans, A.G., 2001. Progressive cracking of a multi-layer system upon thermal cycling. Journal of Applied Mechanics, 68, 513–520.

Begley, M.R., McMeeking, R.M., 1995. Numerical analysis of fiber bridging and fatigue crack growth in metal matrix composite materials. Materials Science and Engineering A 200, 12–21.

Beuth, J.L., 1992. Cracking of thin bonded films in residual tension. International Journal of Solids and Structures 29, 1657–1675.

Beuth, J.L., Klingbeil, N.W., 1996. Cracking of thin films bonded to elastic–plastic substrates. Journal of the Mechanics and Physics of Solids 44, 1411–1428.

Delannay, F., Warren, P., 1991. On crack interaction and crack density in strain-induced cracking of brittle films on ductile substrates. Acta Metallurgica et Materialia 39, 1061–1072.

Ghahremani, F., Shih, C.F., 1992. Corner singularities of three-dimensional plane interface cracks. Journal of Applied Mechanics 59, 61–68.

Hutchinson, J.W., Suo, Z., 1992. Mixed mode cracking in layered materials. In: Hutchinson, J.W., Wu, T.Y. (Eds.), Advances in Applied Mechanics, vol. 29. Academic Press, San Diego, pp. 63–191.

Liu, X.H., Suo, Z., Ma, Q., Fujimoto, H., 2000. Developing design rules to avert cracking and debonding in integrated circuit structures. Engineering Fracture Mechanics 66, 387–402.

Maier, G., 2001. Low-dielectric constant polymers for microelectronics. Progress in Polymer Science 26, 3–65.

Martin, S.J., Godschalx, J.P., Mills, M.E., Shaffer II, E.O., Townsend, P.H., 2000. Development of a low-dielectric-constant polymer for the fabrication of integrated circuit interconnects. Advanced Materials 12, 1769–1778.

Peters, L., 1999. Solving the integration challenges of low-k dielectrics. Semiconductor International, November, pp. 56–60.

Schulze, G.W., Erdogan, F., 1998. Periodic cracking of elastic coatings. International Journal of Solids and Structures 35, 3615–3635.

Thouless, M.D., 1990. Crack spacing in brittle films on ductile substrates. Journal of the American Ceramic Society 73, 2144–2146.